Collective band structures in the γ-soft nucleus ^{135}Nd

W. F. Piel, Jr., C. W. Beausang, D. B. Fossan, L. Hildingsson,* and E. S. Paul
Physics Department, State University of New York at Stony Brook, Stony Brook, New York 11794
(Received 4 November 1986)

The low-lying band structure of ^{135}Nd has been extended to higher spins using the ^{112}Cd(^{27}Al,p3nγ)^{135}Nd and ^{116}Sn(^{24}Mg,2p3nγ)^{135}Nd reactions. Two distinct high-spin structures have been identified. The $\Delta J=1$ band built on the $\nu h_{11/2}[514]\frac{9}{2}^-$ ground state was observed to have a band crossing at $J^\pi=\frac{25}{2}^-$. This band crossing is associated with a loss of the moderate signature splitting found below the backbend. Cranked-shell model calculations suggest that this structure involves the alignment of a pair of $h_{11/2}$ protons and that the loss of signature splitting can be attributed to a shape change from a triaxial shape at low spins to a prolate axial shape above the backbend. A second $\Delta J=1$ band structure with no signature splitting was observed to be built on a $J^\pi=\frac{17}{2}^{(+)}$ state at 1954 keV. Values for the ratios of reduced transition rates $B(M1;I\rightarrow I-1)/B(E2;I\rightarrow I-1)$ and $B(M1;I\rightarrow I-1)/B(E2;I\rightarrow I-2)$ have been extracted from transitions in the two bands. Comparisons with theoretical predictions helped in the identification of the structure of the second $\Delta J=1$ band, which is thought to be based on a $\nu h_{11/2}\otimes\pi h_{11/2}\otimes\pi g_{7/2}$ three-quasiparticle configuration.

I. INTRODUCTION

Nuclear structure calculations[1] predict that the intrinsic shapes of nuclei in the $A=130$ region are soft with respect to γ, the triaxial coordinate in the polar representation of rotating quadrupole shapes. Because of the γ softness, significant shape changes are predicted by cranked-shell model (CSM) calculations for different valence-particle configurations including the alignment of nuclear pairs. This leads to the coexistence of quadrupole structures with different spectroscopic character. Experimental features, such as band crossing frequencies, aligned angular momenta, and signature splittings, can serve as probes of these quadrupole (ϵ,γ) structures.

The strongest shape effects arise from particles in high-j orbitals. The neutron Fermi surface lies near the top of the $h_{11/2}$ shell, where the deformation driving force is to large negative values of γ. Conversely, the proton Fermi surface is near the bottom of the $h_{11/2}$ shell, where the orbitals favor prolate axial symmetry. The protons are thus more susceptible to alignments at lower rotational frequencies, and such $h_{11/2}$ proton alignments have been observed in light Ba and Ce isotopes.[2,3] Both single-quasiparticle configurations, as seen in odd nuclei, and multiquasiparticle configurations, seen in nuclei at high frequencies, influence the nuclear shape. Furthermore, the shape changes are sensitive to the alignment of specific nucleonic pairs. Odd-proton nuclei tend to be axially symmetric, whereas odd-neutron nuclei are expected to be triaxial due to the influence of the valence nucleon. An $h_{11/2}$ neutron would also block any low frequency neutron alignments. Hence, the study of γ-soft odd-N nuclei to high spins is particularly interesting because of triaxiality at low spins, and near axiality at high spins, where quasiprotons can be present in addition to the odd quasineutron.

Odd-neutron nuclei display $h_{11/2}$ bands that are signature split; the amount of splitting is sensitive to the degree of triaxiality. Similarly, the alignment frequencies of specific nucleonic pairs are found to be sensitive to the degree of triaxiality. Thus the study of odd-N nuclei in this mass region can serve as a sensitive probe of the nuclear shape. The goal of the present study is to investigate the level structure of ^{135}Nd in order to observe the rotational properties of this odd-neutron nucleus. Empirical information on electromagnetic transition rates are expected to offer additional constraints on theoretical interpretations of the nuclear structure. The results will be discussed within the formalism of the cranked-shell model including triaxiality using the techniques put forward by Bengtsson and Frauendorf.[4] A semiclassical formalism proposed by Dönau and Frauendorf[5] will be used to discuss the transition probabilities.

The nuclide ^{135}Nd had previously been studied by J. Gizon *et al.*,[6] who used the ^{122}Te(^{16}O,3nγ)^{135}Nd reaction to populate a $\Delta J=1$ negative-parity band of states up to $J^\pi=\frac{19}{2}^-$. More recently, J. van Klinken *et al.*[7] have studied the β^++EC decay of ^{135}Pm to ^{135}Nd (EC denotes electron capture). A preliminary report on the current study has been made.[8] A very recent search in Nd isotopes for gamma rays from the second deformation minimum has been undertaken with the (^{40}Ar,4n) reaction.[9] No significant population of a large-deformation band was observed in the current experiment.

II. EXPERIMENTAL PROCEDURES

Calculations performed with CASCADE along with previous empirical studies in this mass region suggested that fusion-evaporation channels involving either one or two protons would be a better approach to the study of ^{135}Nd than a pure neutron channel. Therefore, the two reactions

^{112}Cd(^{27}Al,p3nγ)^{135}Nd and ^{116}Sn(^{24}Mg,2p3nγ)^{134}Nd were used to study ^{135}Nd with the heavy ion beams produced by the Stony Brook Superconducting LINAC Facility. The cadmium target consisted of 3 mg/cm^2 of ^{112}Cd ($\Delta E = 14$ MeV, 97% enrichment) rolled onto a 60 mg/cm^2 lead backing which served to stop the ^{27}Al beam. The tin target consisted of 2 mg/cm^2 of ^{116}Sn ($\Delta E = 8$ MeV, 96% enrichment) rolled onto a 50 mg/cm^2 lead backing.

The data reported here include γ-ray excitation functions, angular distributions, and γ-γ coincidence measurements. In order to decide on the optimum bombarding energy for each reaction, the γ-ray excitation functions were studied first. Gamma-ray singles spectra were recorded as a function of bombarding energy. From an inspection of the yields of the transition previously assigned to ^{135}Nd, the optimum beam energy for the ^{27}Al beam was found to be 140 MeV, while an energy of 144 MeV was used for subsequent measurements with the ^{24}Mg beam.

The γ-γ coincidence data were recorded using four n-type Ge detectors, each having an efficiency of 25% relative to a 7.6 cm$\times$7.6 cm NaI(Tl) detector for 1.3 MeV γ rays. The detectors were located at $\pm 57°$ and $\pm 136°$ with respect to the beam direction, and at a distance of 14 cm from the target. For the ^{27}Al+^{112}Cd γ-γ coincidence measurements, two of the four detectors utilized bismuth germanate (BGO) anti-Compton shields of the transverse type,[10] while for the ^{24}Mg+^{116}Sn run, BGO shields were used for all four detectors. The coincidence data were event-mode recorded onto magnetic tape for subsequent data analysis.

The tapes were scanned offline on a VAX 11-780 compute to produce a symmetrized 2048$\times$2048 array of E_γ vs E_γ. Background-subtracted gated spectra were generated from this array with gates initially set on known ^{135}Nd transitions. Additional ^{135}Nd transitions could then be identified and used for gates; this process continued in an iterative manner until no additional ^{135}Nd transitions could be found in the spectra. The level scheme of ^{135}Nd that has been deduced from the gated spectra is presented in Fig. 1. Figure 2 displays the sum of several γ-γ coincidence gates from the ^{24}Mg+^{116}Sn data. Although the spectra are complicated by the large number of reaction channels which are open, the suppressed Compton background facilitates the identification of weak transitions.

The γ-ray angular distribution spectra, obtained by ^{27}Al+^{112}Cd at a beam energy of 140 MeV, were recorded by positioning a Ge detector successively at each of four angles with respect to the beam axis: 90°, 120°, 135°, and 152°. Two methods of normalization were used and found to agree to 2.5%. One method used the integrated beam current on the target, and the second employed a fixed Ge detector at 90° as a monitor. The average normalization of the two methods was used to extract A_0, A_2/A_0, and A_4/A_0 values for the ^{135}Nd transitions.

III. RESULTS

In order to obtain information about the multipolarity of each ^{135}Nd transition, the formula

$$W(\theta) = A_0 + A_2 P_2(\theta) + A_4 P_4(\theta)$$

was fitted to the empirical γ-ray intensity function $W(\theta)$, where θ is the angle of the detector measured with respect to the beam axis; A_0, A_2, and A_4 are adjustable parameters, while $P_2(\theta)$ and $P_4(\theta)$ are Legendre polynomials. The results are listed in Table I, where a small correction has been made to each A_2/A_0 and A_4/A_0 ratio for the fi-

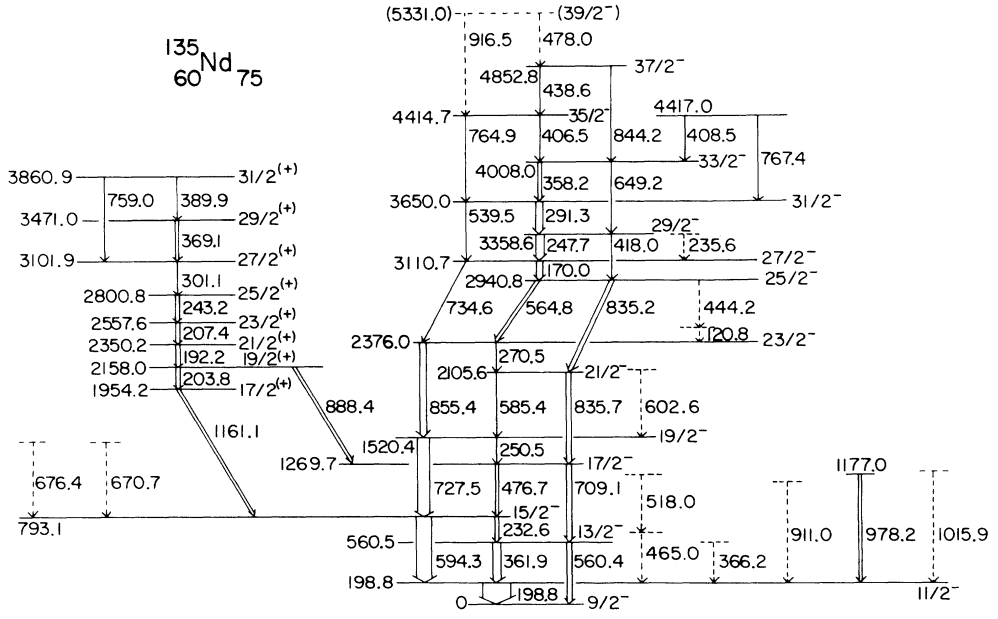

FIG. 1. The proposed level scheme of ^{135}Nd deduced from this work. The γ-ray intensities are indicated by the width of the arrows. Transitions which can only tentatively be placed are indicated by dashed lines.

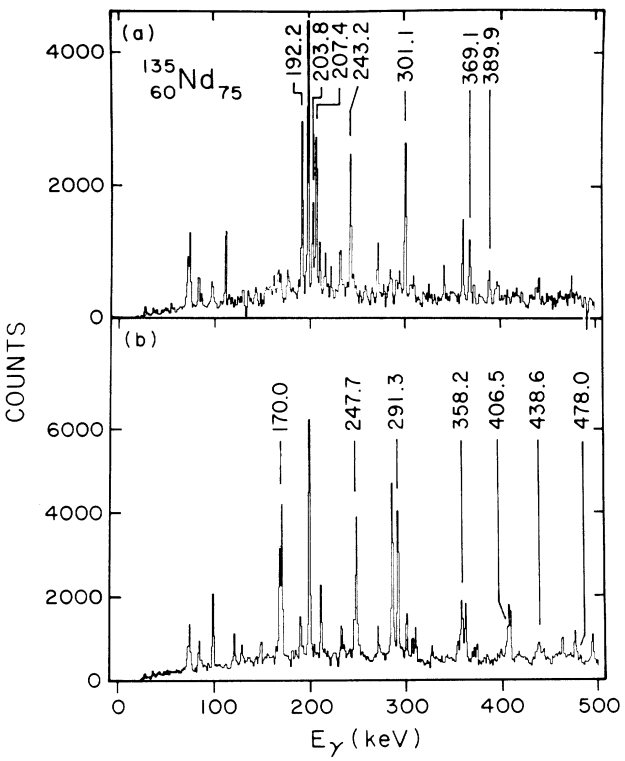

FIG. 2. (a) Summed spectrum of background-subtracted γ-γ coincidence gates set on the four transitions 203.8, 192.2, 207.4, and 243.2 keV. The $\Delta J=1$ intraband transitions above the backbend are labeled with their energies in keV. The unlabeled peaks are either low-lying transitions in ^{135}Nd or contaminating peaks from other nuclides. (b) Similarly for the four transitions 170.0, 247.7, 291.3, and 358.2 keV.

nite detector size. For several transitions, the A_4/A_0 value obtained was unreasonably large; thus for these cases the fit was repeated and just an A_2/A_0 value was extracted by setting A_4 equal to zero. The A_0 values were corrected for the efficiency of the detector and normalized to the $\frac{11}{2}^- \rightarrow \frac{9}{2}^-$ transition. The transition intensities were also carefully determined from γ-γ coincidence data for the ^{24}Mg+^{116}Sn experiment; this analysis made use of both the level scheme shown in Fig. 1 and the calculated internal conversion coefficients of Rösel *et al.*[11] If the intensity of a transition obtained from the ^{24}Mg+^{116}Sn γ-γ analysis was nearly in agreement with the A_0 value listed in Table I for the ^{27}Al+^{112}Cd angular distribution experiment, the A_0 value was listed in the second column of Table I; otherwise, it was assumed that the transition was unresolved in singles spectra and the intensity obtained from coincidence data was listed.

The spin and parity assignments shown in Fig. 1 are straightforward for the levels proposed to have negative parity up through the $\frac{37}{2}^-$ level at 4852.8 keV. The lower spin levels up through the $\frac{19}{2}^-$ have previously been reported by Gizon *et al.*[6] using the (^{16}O,3nγ) reaction and are in agreement with their assignments. The A_2/A_0 values listed in Table I for each of the $\Delta J=2$ transitions between negative parity levels are generally large and positive, and the A_4/A_0 value are small and negative, as expected for stretched $E2$ assignments. The results for the $E2$ transitions were used to obtain average values for the alignment parameters: $\alpha_2=0.86\pm0.07$ and $\alpha_4=0.50\pm0.16$. These two parameters were then used to determine the $E2/M1$ mixing ratio δ for several of the $\Delta J=1$ transitions above the $\frac{15}{2}^-$ level. For the three $\Delta J=1$ transitions below this level, smaller parameter values were utilized. The uncertainties in the mixing ratios, listed in the last column of Table I, take into account the uncertainties in the alignment. The mixing ratios extracted for the five lowest $\Delta J=1$ transitions are negative.

Also shown to the left of Fig. 1 is a side cascade feeding into the main cascade at the $\frac{15}{2}^-$ and $\frac{17}{2}^-$ levels through the 1161.1 and 888.4 keV transitions, respectively. This sideband is consistent with a cascade of $\Delta J=1$ transitions, although only one $E2$ crossover transition could be found. The parity of this band was not determined since the A_2/A_0 value for the 1161.1 keV transition is consistent with a stretched dipole assignment, while a value for the 888.4 keV transition was not obtained.

Several additional transitions are shown in Fig. 1; the placement of most of these could only tentatively be made. The ordering of the 444.2 and 120.8 keV transitions, connecting the $\frac{23}{2}^-$ and $\frac{25}{2}^-$ levels, could not be determined; therefore the level between them is dashed in Fig. 1. We remark that the 518.0, 670.7, and 1015.9 keV transitions were also listed by Gizon *et al.*,[6] but not placed in their level scheme. Several of the low-lying transitions in Fig. 1 may be significantly populated by the β^++EC decay of 0.9 min ^{135}Pm, which was also produced by the bombardments.

The empirical mixing ratios, discussed above, together with the γ-ray transition intensities listed in Table I, can be used to calculate $B(M1;I\rightarrow I-1)/B(E2;I\rightarrow I-1)$ ratios; these are summarized in Fig. 3. There is a general increase in this ratio up to $J^\pi=\frac{27}{2}^-$, with a possible decrease at higher spins; no obvious signature dependence can be seen. The transition intensities listed in Table I also yield $B(M1;I\rightarrow I-1)/B(E2;I\rightarrow I-2)$ ratios as shown in Fig. 4. A small signature dependence is seen at low spin, while an increase by a factor of 6 in the average value above $J=\frac{29}{2}$ is found. These data are expected to provide severe restrictions on theoretical interpretations of the structures evident in Fig. 1. The calculated curves shown in Figs. 3 and 4 are based on a semiclassical model[5] and are discussed below.

IV. DISCUSSION

Following standard notation, the lowest negative parity neutron single-quasiparticle states are labeled a, b, c, and d. The lowest positive parity neutron states are labeled e, f, ... Similarly, the lowest negative parity proton states are labeled A, B, C, and D, and the lowest positive parity proton states are labeled E, F, ... The Nilsson single-particle systematics at a quadrupole deformation $\epsilon_2=0.2$ are used to assign these levels. Table II shows such an assignment. The lower energy, or favored, signature component of all the Nilsson levels considered is the $\alpha=-\frac{1}{2}$ component, in accordance with the relation[1] $\alpha=j \bmod 2$,

TABLE I. Transitions in ^{135}Nd produced by 140 MeV ^{27}Al+^{112}Cd. The relative γ-ray intensities have been corrected for the efficiency of the Ge detector, and the A_2/A_0 and A_4/A_0 values have been corrected for the finite solid angle. The $E2/M1$ mixing ratios δ are listed in the last column for several transitions.

E_γ (keV)	Relative intensity	A_2/A_0	A_4/A_0	Assignment
120.76±0.20[a]	4.1±0.1	−0.29 ±0.06	−0.16 ±0.09	($\rightarrow \frac{23}{2}^-$)
170.05±0.20[a]	20.6±1.3[a]	−0.212±0.013[d]	−0.018±0.023[d]	$\frac{27}{2}^- \rightarrow \frac{25}{2}^-$
				$\delta = +0.012 \pm 0.041$
192.24±0.20	16.7±0.4	−0.299±0.023	−0.056±0.036	$\frac{21}{2}^{(+)} \rightarrow \frac{19}{2}^{(+)}$
				$\delta = -0.032 \pm 0.034$
198.82±0.15	≡100.0±0.7[f]	−0.476±0.016[d,f]	−0.010±0.027[d,f]	$\frac{11}{2}^- \rightarrow \frac{9}{2}^-$
				$\delta = -0.22 \pm 0.07$
203.85±0.25[a]	7.6±0.9[a]	c	c	$\frac{19}{2}^{(+)} \rightarrow \frac{17}{2}^{(+)}$
207.45±0.25[a]	14.0±2.0[a]	c	c	$\frac{23}{2}^{(+)} \rightarrow \frac{21}{2}^{(+)}$
232.61±0.20	12.9±0.9[a]	−0.41 ±0.06[a]	−0.09 ±0.09[d]	$\frac{15}{2}^- \rightarrow \frac{13}{2}^-$
				$\delta = -0.13 \pm 0.07$
235.63±0.30	6.7±0.3	−0.49 ±0.09	+0.04 ±0.13	($\rightarrow \frac{27}{2}^-$)
243.20±0.20	12.7±2.1[a]	−0.345±0.021[d]	−0.043±0.033[d]	$\frac{25}{2}^{(+)} \rightarrow \frac{23}{2}^{(+)}$
				$\delta = -0.065 \pm 0.035$
247.74±0.25[a]	28.6±3.9[a]	−0.366±0.017[d]	−0.041±0.027[d]	$\frac{29}{2}^- \rightarrow \frac{27}{2}^-$
				$\delta = -0.079 \pm 0.037$
250.5 ±0.5[a]	4.3±0.5[a]	−0.54 ±0.05[d]	+0.06 ±0.07[d]	$\frac{19}{2}^- \rightarrow \frac{17}{2}^-$
				$\delta = -0.19 \pm 0.08$
270.5 ±0.5[a]	≈1	c	c	$\frac{23}{2}^- \rightarrow \frac{21}{2}^-$
291.34±0.20	23.8±0.3	−0.437±0.021	+0.040±0.032	$\frac{31}{2}^- \rightarrow \frac{29}{2}^-$
				$\delta = -0.121 \pm 0.038$
301.13±0.20[a]	6.8±1.9[a]	c	c	$\frac{27}{2}^{(+)} \rightarrow \frac{25}{2}^{(+)}$
358.22±0.25[a]	13.1±1.8[a]	−0.303±0.021[b]	≡0	$\frac{33}{2}^- \rightarrow \frac{31}{2}^-$
				$\delta = -0.02 \pm 0.13$[e]
361.88±0.15	30.9±0.4[f]	−0.57 ±0.05[f]	−0.03 ±0.08[f]	$\frac{13}{2}^- \rightarrow \frac{11}{2}^-$
				$\delta = -0.89 \pm 0.63$
366.22±0.25[a]	3.3±0.8[a]	c	c	($\rightarrow \frac{11}{2}^-$)
369.12±0.25[a]	12.7±0.2	−0.50 ±0.05	−0.06 ±0.07	$\frac{29}{2}^{(+)} \rightarrow \frac{27}{2}^{(+)}$
				$\delta = -0.16 \pm 0.06$
389.93±0.25	3.2±0.7[a]	−0.044±0.029[b]	≡0	$\frac{31}{2}^{(+)} \rightarrow \frac{29}{2}^{(+)}$
				$\delta = +0.112 \pm 0.029$
406.5 ±0.5[a]	6.8±1.3[a]	−0.59 ±0.06	−0.05 ±0.08	$\frac{35}{2}^- \rightarrow \frac{33}{2}^-$
				$\delta = -0.25 \pm 0.15$[e]
408.5 ±0.5[a]	5.1±1.6[a]	c	c	$\rightarrow \frac{33}{2}^-$
418.0 ±0.5[a]	6.0±1.2[a]	c	c	$\frac{29}{2}^- \rightarrow \frac{25}{2}^-$
438.6 ±0.5[a]	4.2±1.4[a]	−0.60 ±0.05[b,d]	≡0	$\frac{37}{2}^- \rightarrow \frac{35}{2}^-$
				$\delta = -0.26 \pm 0.15$[e]
444.19±0.35	3.3±0.2	+0.68 ±0.13	+0.01 ±0.17	($\frac{25}{2}^- \rightarrow$)
465.0 ±0.6[a]	4.1±1.1[a]	c	c	($\rightarrow \frac{11}{2}^-$)
476.70±0.25[a]	13.9±1.4[a]	−0.383±0.023[b,d]	≡0	$\frac{17}{2}^- \rightarrow \frac{15}{2}^-$
				$\delta = -0.09 \pm 0.11$
478.0 ±0.5[a]	1.7±1.3[a]	c	c	($\frac{39}{2}^-$) $\rightarrow \frac{37}{2}^-$
518.04±0.20	6.7±0.9[a]	c	c	($\rightarrow$663.8 keV)
539.48±0.30[a]	3.0±0.7[a]	c	c	$\frac{31}{2}^- \rightarrow \frac{27}{2}^-$
560.35±0.20	18.9±0.3	+0.247±0.030	+0.004±0.045	$\frac{13}{2}^- \rightarrow \frac{9}{2}^-$
564.79±0.20	14.3±2.2[a]	−0.272±0.023[d]	≡0	$\frac{25}{2}^- \rightarrow \frac{23}{2}^-$
				$\delta = -0.02 \pm 0.07$
585.38±0.25[a]	5.2±1.2[a]	−0.23 ±0.06[d]	−0.01 ±0.08[d]	$\frac{21}{2}^- \rightarrow \frac{19}{2}^-$
				$\delta = 0.00 \pm 0.06$
594.31±0.20	51.5±1.1	+0.320±0.015	−0.073±0.026	$\frac{15}{2}^- \rightarrow \frac{11}{2}^-$

TABLE I. (*Continued*).

E_γ (keV)	Relative intensity	A_2/A_0	A_4/A_0	Assignment
602.6 ±0.5[a]	6.1±1.3[a]	c	c	$(\rightarrow \frac{19}{2}^-)$
649.16±0.30[a]	3.0±1.1[a]	+0.02 ±0.07[d]	+0.04 ±0.10[d]	$\frac{33}{2}^- \rightarrow \frac{29}{2}^-$
670.66±0.40[a]	6.2±0.9	−0.05 ±0.05	+0.03 ±0.07	$(\rightarrow \frac{15}{2}^-)$
676.36±0.40[a]	3.8±1.2[a]	c	c	$(\rightarrow \frac{15}{2}^-)$
709.10±0.20	18.5±1.5	+0.387±0.025[d]	−0.089±0.037[d]	$\frac{17}{2}^- \rightarrow \frac{13}{2}^-$
727.48±0.15	40.1±0.5	+0.332±0.024	−0.097±0.039	$\frac{19}{2}^- \rightarrow \frac{15}{2}^-$
734.65±0.35[a]	3.4±2.3[a]	+0.45 ±0.07[d]	−0.06 ±0.09[d]	$\frac{27}{2}^- \rightarrow \frac{23}{2}^-$
758.99±0.30	4.8±0.2	+0.37 ±0.11	+0.02 ±0.15	$\frac{31}{2}^{(+)} \rightarrow \frac{27}{2}^{(+)}$
764.9 ±0.5[a]	3.1±1.6[a]	+0.07 ±0.07[d]	+0.04 ±0.10[d]	$\frac{35}{2}^- \rightarrow \frac{31}{2}^-$
767.41±0.30	3.9±0.2	−0.51 ±0.13	+0.05 ±0.18	$\rightarrow \frac{31}{2}^-$
835.18±0.40[a]	18.6±2.4[a]	+0.251±0.023	+0.012±0.035	$\frac{25}{2}^- \rightarrow \frac{21}{2}^-$
835.7 ±0.5[a]	13.6±3.2[a]			$\frac{21}{2}^- \rightarrow \frac{17}{2}^-$
844.23±0.40[a]	3.4±1.7[a]	c	c	$\frac{37}{2}^- \rightarrow \frac{33}{2}^-$
855.40±0.30	19.7±0.2	+0.307±0.026	+0.004±0.039	$\frac{23}{2}^- \rightarrow \frac{19}{2}^-$
888.42±0.30[a]	8.0±1.0[a]	c	c	$\frac{19}{2}^{(+)} \rightarrow \frac{17}{2}^-$
911.02±0.40[a]	2.4±0.9[a]	c	c	$(\rightarrow \frac{11}{2}^-)$
916.52±0.40[a]	1.4±1.1[a]	c	c	$(\frac{39}{2}^-) \rightarrow \frac{35}{2}^-$
978.18±0.25	11.0±0.2	+0.15 ±0.06	0.01 ±0.08	$\rightarrow \frac{11}{2}^-$
1015.9 ±0.5[a]	5.8±1.0[a]	c	c	$(\rightarrow \frac{11}{2}^-)$
1161.10±0.25	9.0±0.2	−0.21 ±0.06	+0.07 ±0.08	$\frac{17}{2}^{(+)} \rightarrow \frac{15}{2}^-$

[a]Energy or intensity better obtained from γ-γ coincidence spectra produced by 144 MeV ^{24}Mg+^{116}Sn.
[b]A_2/A_0 value found by assuming $A_4=0$.
[c]Transitions unresolved from another transition.
[d]This value includes a small contribution from an unresolved transition.
[e]A range of values with $|\delta| > 1$ also is allowed.
[f]These values are perturbed due to a component from the β^+ + EC decay of 0.9 min ^{135}Pm. The mixing ratio has been corrected. No correction has been made for a 6% intensity component to the 198.8 keV transition due to an unresolved $\Delta J = 1$ transition in ^{136}Pm.

which gives the favored signature for a j shell. The definition of the parameter γ is taken to be consistent with the Lund convention;[12] a value of $+60°$ represents rotation of an oblate shape about the symmetry axis and is noncollective, while a value of $-60°$ represents the collective rotation of an oblate shape about one of the long axes.

Experimental Routhians of the bands observed in ^{135}Nd are shown in Fig. 5. A frequency-dependent moment of inertia reference

$$\mathcal{I}_{\text{ref}} = \mathcal{I}_0 + \omega^2 \mathcal{I}_1$$

has been subtracted from the data with the Harris[13] parameters taken as the average of those obtained from a fit to the ground-state bands of the neighboring even-even ^{134,136}Nd isotopes. These values are $\mathcal{I}_0 = 6.6\hbar^2$ MeV^{-1} and $\mathcal{I}_1 = 86\hbar^4$ MeV^{-3}. The total aligned spin I_x of the bands is shown in Fig. 6 as a function of frequency. Also shown in Fig. 6 are the alignments i_x which were obtained by subtracting the frequency-dependent reference from the total aligned spin I_x of the bands.

A. The neutron $h_{11/2}[514]\frac{9}{2}^-$ ground-state band

In the ground state of ^{135}Nd the odd neutron occupies level b, which is the signature $\alpha = \frac{1}{2}$ component of the $h_{11/2}[514]\frac{9}{2}^-$ Nilsson orbital. A rotational band is seen built on this state consisting of three $E2$ transitions up to spin $J^\pi = \frac{21}{2}^-$. In addition, a similar band is built on the level at 199 keV, which is the opposite signature state a of the $[514]\frac{9}{2}^-$ orbital. $M1$ transitions are seen connecting these two signature components. The two bands are also displaced with respect to each other and this shows up as a signature splitting $[E_b(\omega) - E_a(\omega) > 0]$ as seen in the Routhian plot of Fig. 5. The splitting is in excess of 100 keV and increases with rotational frequency. At $\hbar\omega \simeq 0.32$ MeV both bands built on the a and b states show a gain in their alignment $\Delta i_x \sim 10\hbar$, as can be seen in Fig. 6. Such a backbend can be understood as being due to the alignment of the lowest pair of $h_{11/2}$ protons in the $[541]\frac{3}{2}^-$ orbital. This alignment is referred to as the AB crossing. A similar alignment of the first two $h_{11/2}$ neu-

TABLE II. Level assignments for ^{135}Nd taken from Nilsson single-particle systematics at a deformation $\epsilon=0.2$.

$\nu h_{11/2}$	$[514]\frac{9}{2}^-$	$\alpha=-\frac{1}{2}$	a
		$\alpha=+\frac{1}{2}$	b
$\nu h_{11/2}$	$[523]\frac{7}{2}^-$	$\alpha=-\frac{1}{2}$	c
		$\alpha=+\frac{1}{2}$	d
$\nu d_{3/2}$	$[400]\frac{1}{2}^+$	$\alpha=-\frac{1}{2}$	e
		$\alpha=+\frac{1}{2}$	f
$\pi h_{11/2}$	$[514]\frac{3}{2}^-$	$\alpha=-\frac{1}{2}$	A
		$\alpha=+\frac{1}{2}$	B
$\pi g_{7/2}$	$[413]\frac{5}{2}^+$	$\alpha=-\frac{1}{2}$	E
		$\alpha=+\frac{1}{2}$	F

trons, the *ab* crossing, is blocked in both signature components of the ground-state rotational band due to the occupancy of either state *a* or state *b*. The next allowed $h_{11/2}$ neutron alignments, the *bc* and *ad* crossings, occur at substantially higher frequencies.

Standard cranked-shell model[4] calculations, with parameters $\epsilon_2=0.2$, $\epsilon_4=0.0$, $\gamma=0°$, and $\Delta_n=\Delta_p=1.2$ MeV, predict the proton *AB* alignment to occur at a frequency $\hbar\omega=0.28$ MeV, which is somewhat lower than the experimental value obtained from the Routhians of Fig. 5. Such calculations are relatively insensitive to moderate changes in the parameters ϵ_2, ϵ_4, Δ_n, and Δ_p. However, nuclei in this mass region are known to be soft with respect to the γ deformation and moderate changes in γ can greatly in-

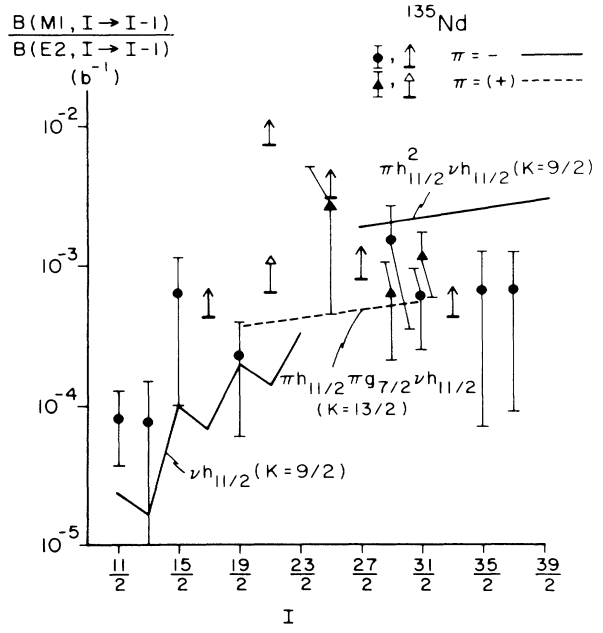

FIG. 3. The empirical ratios of reduced transition rates for ^{135}Nd utilizing the nonstretched *E*2 transitions. The bottom of each arrow represents an empirical lower limit. The curves are semiclassical predictions for the various configurations shown.

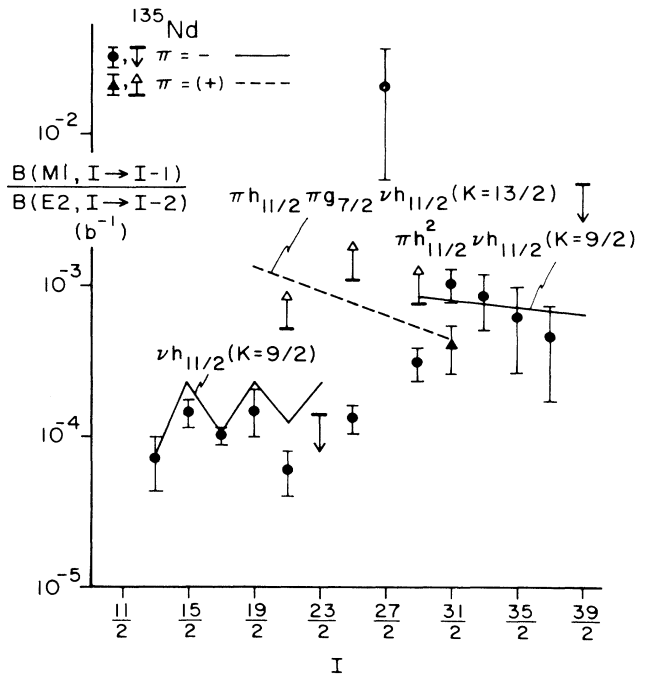

FIG. 4. The empirical ratios of reduced transition rates for ^{135}Nd utilizing the stretched *E*2 transitions. The bottom (top) of each upward (downward) pointing arrow represents an empirical lower (upper) limit. The curves are theoretical predictions for the various configurations shown.

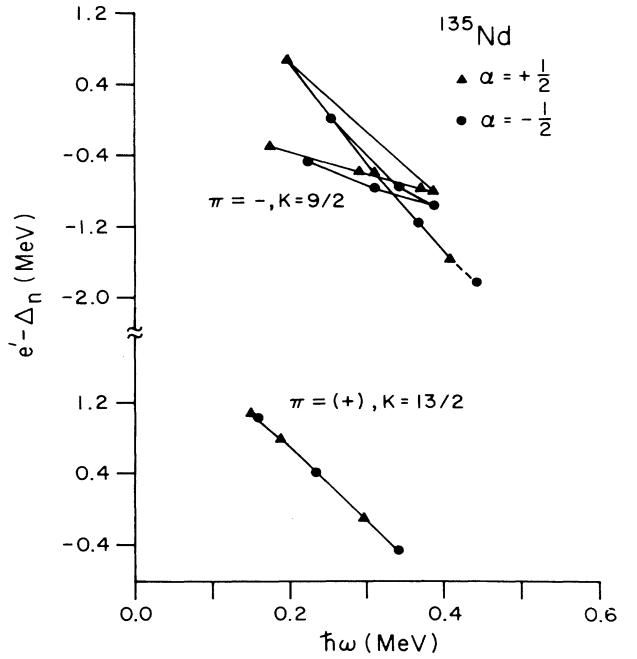

FIG. 5. Experimental Routhians of the bands in ^{135}Nd. A reference has been subtracted with Harris parameters $\mathcal{I}_0=6.6\hbar^2$ MeV^{-1} and $\mathcal{I}_1=86\hbar^4$ MeV^{-3}, which are average values of those fitted to the ground-state bands of the even-even neighbors ^{134,136}Nd. The curves are calculated using $K=\frac{9}{2}$ for the negative parity levels and $K=\frac{13}{2}$ for the positive parity levels.

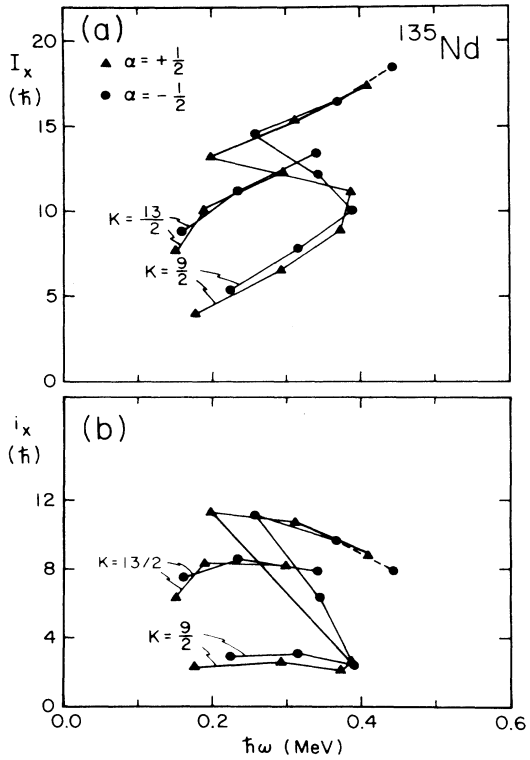

FIG. 6. The total aligned angular momenta I_x and alignment i_x of the bands in ^{135}Nd shown as a function of rotational frequency. The curves are calculated using $K=\frac{9}{2}$ for the negative parity levels and $K=\frac{13}{2}$ for the positive parity levels.

fluence the frequencies at which various particles decouple. Figure 7 shows how the crossing frequencies for proton and neutron $h_{11/2}$ pairs change as a function of γ. These curves were obtained from standard CSM calculations by fixing γ at a particular value and examining the single-quasiparticle levels as a function of rotational frequency to extract the various crossing frequencies. The values of γ associated with the curves in Fig. 7 are thus interpreted as estimates of γ occurring in the zero-quasiparticle or one-quasiparticle band just below the crossing frequency. The alignment of either neutrons or protons is expected to greatly influence the γ deformation above the crossing.[14] The first two possible alignments in the ground-state band are the proton *AB* and neutron *bc* crossings, the neutron *ab* crossing being blocked. The proton *AB* crossing, which is predicted to occur at $\hbar\omega=0.28$ MeV at $\gamma=0°$, is seen to rise sharply in frequency as γ becomes more negative. In fact, at $\gamma\sim-20°$ the experimental crossing frequency $\hbar\omega_{AB}=0.32$ MeV is reproduced. It should also be noted that the neutron *bc* crossing frequency is always above the experimental value in the whole range of γ, i.e., $-120°<\gamma<60°$. Hence the band crossing is attributed to $h_{11/2}$ protons and the experimental crossing frequency can be understood if the nucleus possesses a triaxial deformation of $\gamma\sim-20°$ just below the backbend.

Above the crossing the three-quasiparticle states *ABa*

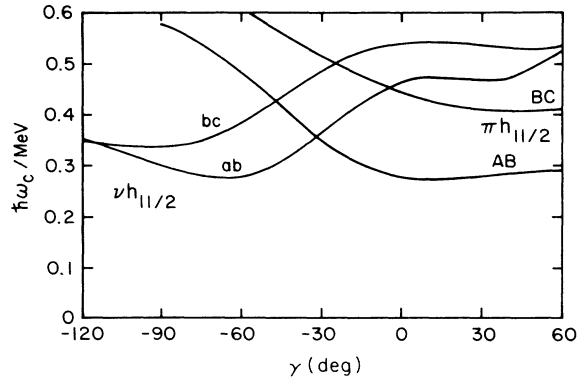

FIG. 7. The calculated decoupling frequencies of $h_{11/2}$ protons (*AB* and *BC*) and $h_{11/2}$ neutrons (*ab* and *bc*) as a function of the γ deformation.

and *ABb* are somewhat different than the one-quasiparticle states *a* and *b* below the crossing. Indeed, the relative strength of the *M*1 transitions is increased at the expense of the *E*2 crossovers, as shown in Fig. 4. This results from the changed configurations and because the signature splitting between the two components has fallen to, or very close to, zero. Calculations of the relative $B(M1)/B(E2)$ reduced transition rates for the $\nu h_{11/2}\otimes(\pi h_{11/2})^2$ configuration, using the semiclassical formalism of Dönau and Frauendorf,[5] are in quantitative agreement with the empirical values shown in Figs. 3 and 4. The calculated negative sign of the $E2/M1$ mixing ratio δ for this configuration is also consistent with experiment.

The experimental Routhians of Fig. 5 show zero splitting above the backbend. One mechanism for the disappearance of the signature splitting is that the nucleus becomes axial, i.e., $\gamma=0°$, above the backbend. Figure 8 shows the calculated $h_{11/2}$ neutron and proton quasiparticle levels as a function of γ. Three important features should be noted. First, the proton *A* and *B* levels tend to drive the nuclear shape towards $\gamma=0°$; i.e., tend to stabi-

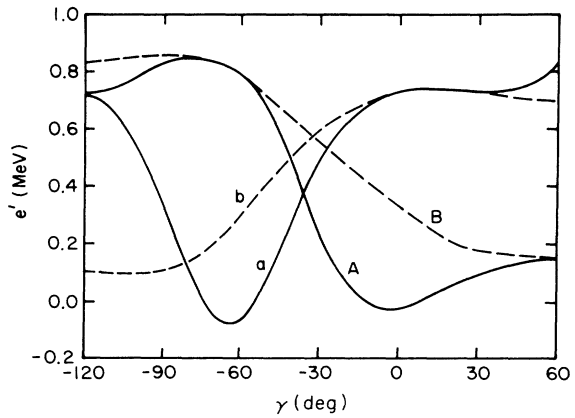

FIG. 8. Calculated proton (*A* and *B*) and neutron (*a* and *b*) $h_{11/2}$ quasiparticle levels as a function of the γ deformation. The calculations were performed at $\hbar\omega=250$ keV.

lize the prolate axial deformation of the core. Many examples of prolate $h_{11/2}$ proton bands are known in this mass region, where the odd proton is weakly coupled to a prolate core. Second, the neutron a and b levels tend to drive the nuclear shape to large negative values of γ close to $\gamma=-60°$, which represents collective oblate rotation about one of the long axes. Third, it can be seen that the energy difference or signature splitting between the levels changes as a function of γ; in particular, the ab splitting is zero at $\gamma=0°$.

Figure 8 shows the single-quasiparticle energies in the rotating frame. It is more appropriate to discuss the total energy of the nucleus in the rotating frame and this transformation is achieved by adding a γ-dependent reference to the single-quasiparticle Routhians as proposed by Frauendorf and May.[14] Thus the total Routhian is

$$E'(\omega,\gamma)=e'(\omega,\gamma)+E'_{\rm ref}(\omega,\gamma) ,$$

with reference

$$E'_{\rm ref}(\omega,\gamma)=\tfrac{1}{2}V_{po}\cos 3\gamma-\tfrac{2}{3}\omega^2(\mathscr{I}_0+\tfrac{1}{2}\omega^2\mathscr{I}_1)\cos^2(\gamma+30°) .$$

V_{po} is related to the energy difference between prolate and oblate shapes and is taken as $V_{po}=-0.9$ MeV for the $h_{11/2}$ levels in accordance with Aryaeinejad *et al.*[15] The Harris parameters were those used in constructing the experimental Routhians of Fig. 5. Such total Routhians, calculated at $\hbar\omega=250$ keV, are shown in Fig. 9 for several configurations, including the one- and three-quasiparticle portions of the $\nu h_{11/2}$ band. The one-quasiparticle levels a and b are relatively flat and show minima at negative values of γ, where there is a moderate signature splitting. The three-quasiparticle levels *ABa* and *ABb* have minima close to $\gamma=0°$, where the signature splitting is zero. Hence the loss of signature splitting observed in the $\nu h_{11/2}$ band above the crossing can be understood as being due to the alignment of the AB protons which subsequently drive the γ deformation towards $\gamma=0°$. The increase of the signature splitting with frequency observed below the backbend is due to the deformation driving effect of the odd $h_{11/2}$ neutron, with γ becoming more negative as the frequency increases, and reaches a value $\gamma\sim-20°$ at the backbend.

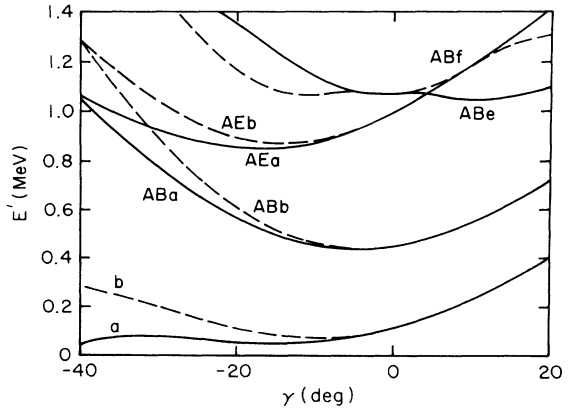

FIG. 9. Calculated total Routhians as a function of the γ deformation for the possible quasiparticle configurations seen in ^{135}Nd. The calculations were performed at $\hbar\omega=250$ keV.

A closer inspection of the levels a and b as shown in Fig. 9 shows that they possess minima at different values of γ. A similar inspection of the experimental Routhians of Fig. 5 yields slightly different crossing frequencies for the two signatures components of the $\nu h_{11/2}$ band. In fact, $\hbar\omega_{AB}(a)=0.336$ MeV, whereas $\hbar\omega_{AB}(b)=0.318$ MeV. The difference, in this case, $\Delta\hbar\omega_{AB}=18$ keV, has been interpreted[14] as evidence for a different value of nuclear triaxiality depending on which signature component is occupied. Figure 9 shows a minimum at a more negative value of γ for the neutron a level when compared to the neutron b level. Such a difference would indeed lead to a higher band crossing frequency observed in the band built on the state a and is in qualitative agreement with experiment. The calculated signature splitting between the two components at $\hbar\omega=250$ keV,

$$\Delta E'=E'_b(\omega,\gamma=-8°)-E'_a(\omega,\gamma=-16°)=25 \text{ keV} ,$$

obtained from Fig. 9, is somewhat smaller than the experimental value of 100 keV.

B. The $\Delta J=1$ sideband

The sideband shown to the left of Fig. 1 is similar to the three-quasiparticle portion of the $\nu h_{11/2}$ band in that the signature splitting is again zero and that the $M1$ transitions are stronger than the $E2$ crossovers. The alignment of this band, as shown in Fig. 6, is $(3-4)\hbar$ lower than the corresponding three-quasiparticle negative parity levels. The parity of the sideband was not determined experimentally, but theoretical considerations favor positive parity, as discussed below.

One possible structure of the sideband is a three-quasiparticle configuration with the odd neutron occupying a low-j orbital and coupled to a pair of aligned particles. Nilsson systematics suggest as a candidate the $d_{3/2}[400]\frac{1}{2}^+$ orbital. The two signature components of this orbital are referred to as e and f as in Table II. It is expected from energy considerations that the protons decouple preferentially to the neutrons, although in this case the neutron ab crossing is not blocked. However, a neutron alignment would tend to drive the deformation towards $\gamma=-60°$, where there is a significant signature splitting between the levels *abe* and *abf*. These levels are also calculated to lie at a high excitation energy and therefore this structure can be ruled out. The sideband could then be based on a $\nu d_{3/2}\otimes(\pi h_{11/2})^2$ configuration with $\gamma\sim0°$ and no signature splitting between the components *ABe* and *ABf* as shown in Fig. 9.

An alternative structure for the sideband is the three-quasiparticle configuration $\nu h_{11/2}\otimes\pi h_{11/2}\otimes\pi g_{7/2}$. This structure involves a decoupled $h_{11/2}$ proton, a strongly coupled $g_{7/2}$ proton, and a strongly coupled $h_{11/2}$ neutron. In the standard notation the sideband is built on the configurations *AEa* and *AEb*. These configurations are also shown in Fig. 9 and are lower in energy than the *ABe* and *ABf* levels. The minima of the levels *AEa* and *AEb* are at a negative value of γ with a small signature splitting, whereas experimentally no signature splitting was

observed. However, this proposed structure for the sideband is the more likely for two reasons.

First, strong $M1$ transitions would be expected for this configuration because of the two strongly coupled particles which have a relatively large spin component K, and hence a large component of the magnetic dipole moment perpendicular to the total spin **I** of the nucleus. The reduced $M1$ transition probability $B(M1)$ is proportional to the square of this perpendicular component $\mu_\perp$ of the magnetic dipole moment μ. Calculations using the semiclassical formalism of Dönau and Frauendorf[5] yield $B(M1)/B(E2)$ ratios for the $\nu h_{11/2}\otimes\pi h_{11/2}\otimes\pi g_{7/2}$ configuration (AEa and AEb) in quantitative agreement with the empirical values shown in Figs. 3 and 4. A K value of $\frac{13}{2}$ gave the best fit to the data. In contrast, the $B(M1)/B(E2)$ ratios calculated for the $\nu d_{3/2}\otimes(\pi h_{11/2})^2$ configuration (ABe and ABf) are ~ 70 times smaller than experiment, because of a small K value and a small component $\mu_\perp$ of the magnetic dipole moment. The empirical negative $E2/M1$ mixing ratios extracted from transitions in the sideband are also consistent with a structure based on the $\nu h_{11/2}\otimes\pi h_{11/2}\otimes\pi g_{7/2}$ configuration.

Secondly, 5^- states based on the AE configuration have been observed in the neighboring even-even ^{134,136}Nd isotopes[16] at excitation energies similar to the $\frac{17}{2}^+$ level in ^{135}Nd. Figure 10 shows a comparison of these sidebands seen in the ^{134,135,136}Nd isotopes. It appears likely that the sideband in ^{135}Nd involves the odd $h_{11/2}$ neutron coupled to the AE states of the even-even neighbors.

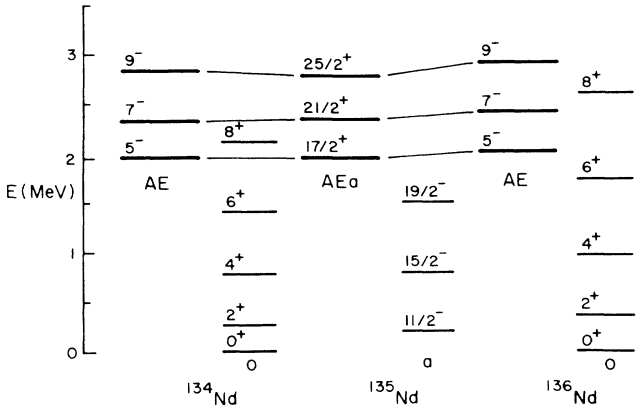

FIG. 10. Comparison of the sidebands observed in the ^{134,135,136}Nd nuclei as discussed in the text.

V. CONCLUSIONS

The nucleus ^{135}Nd has been found to be an example of a γ-soft nucleus in the $A=130$ mass region. At low spins the nucleus is triaxial due to the influence of an odd neutron near the top of the $h_{11/2}$ shell. At higher spins a band crossing due to protons has been observed. The alignment of a pair of protons from the bottom of the $h_{11/2}$ shell drives the nucleus to prolate axial shapes at the higher spins. The signature splitting due to the odd neutron is observed to disappear above the band crossing because of this shape change to $\gamma\sim 0°$. A second band with no signature splitting and strong $M1$ transitions has also been observed. Comparison of the experimental ratios of reduced transition probabilities, $B(M1)/B(E2)$, with theoretical predictions suggests that the sideband contains a structure related to the two-quasiparticle states seen in the neighboring even-even Nd isotopes.

This work was supported in part by the National Science Foundation.

*Present address: Research Institute of Physics, S 104 05 Stockholm 50, Sweden.

[1]Y. S. Chen, S. Frauendorf, and G. A. Leander, Phys. Rev. C **28**, 2427 (1983).
[2]D. Ward, H. Bertschat, P. A. Butler, P. Colombani, R. M. Diamond, and F. S. Stephens, Phys. Lett. **56B**, 139 (1975).
[3]P. J. Nolan, D. M. Todd, P. J. Smith, D. J. G. Love, P. J. Twin, O. Andersen, J. D. Garrett, G. B. Hagemann, and B. Herskind, Phys. Lett. **108B**, 269 (1982).
[4]R. Bengtsson and S. Frauendorf, Nucl. Phys. **A327**, 139 (1979).
[5]F. Dönau and S. Frauendorf, in *Proceedings of the Conference on High Angular Momentum Particles of Nuclei,* Oak Ridge, 1982, edited by N. R. Johnson (Harwood-Academic, New York, 1983), p. 143; F. Dönau, NBI-ZFK Report 85-36, 1986.
[6]J. Gizon, A. Gizon, M. R. Maier, R. M. Diamond, and F. S. Stephens, Nucl. Phys. **A222**, 557 (1974).
[7]J. van Klinken and S. J. Feenstra, Phys. Rev. C **12**, 2111 (1975).
[8]W. F. Piel, Jr., C. W. Beausang, D. B. Fossan, L. Hildingsson, and E. S. Paul, Bull. Am. Phys. Soc. **31**, 836 (1986).
[9]E. M. Beck, private communication.
[10]L. Hildingsson, C. W. Beausang, D. B. Fossan, W. F. Piel, Jr., A. P. Byrne, and G. D. Dracoulis, Nucl. Instrum. Methods **A252**, 91 (1986).
[11]F. Rösel, H. M. Fries, K. Adler, and H. C. Pauli, At. Data Nucl. Data Tables **21**, 91 (1978).
[12]G. Andersson, S. E. Larsson, G. Leander, P. Möller, S. G. Nilsson, I. Ragnarsson, S. Åberg, R. Bengtsson, J. Dudek, B. Nerlo-Pomorska, K. Pomorski, and Z. Szynmański, Nucl. Phys. **A268**, 205 (1976).
[13]S. M. Harris, Phys. Rev. **138**, B509 (1965).
[14]S. Frauendorf and F. R. May, Phys. Lett. **125B**, 245 (1983).
[15]R. Aryaeinejad, D. J. G. Love, A. H. Nelson, P. J. Nolan, P. J. Smith, D. M. Todd, and P. J. Twin, J. Phys. G **10**, 955 (1984).
[16]C. W. Beausang, D. B. Fossan, R. Ma, E. S. Paul, W. F. Piel, Jr., S. Shi, P. K. Weng, and N. Xu (unpublished).